 CMC, vol.23, no.3, pp.265-285, 2011

A New Discrete-Layer Finite Element for Electromechanically Coupled Analyses of Piezoelectric Adaptive Composite Structures

M. Al-Ajmi[1] **and A. Benjeddou**[2]

Abstract: A new discrete layer finite element (DLFE) is presented for electromechanically coupled analyses of moderately thick piezoelectric adaptive composite plates. The retained kinematics is based on layer-wise first-order shear deformation theory, and considers the plies top and bottom surfaces in-plane displacements and the plate transverse deflection as mechanical unknowns. The former are assumed in-plane Lagrange linear, while the latter is assumed in-plane full (Lagrange) quadratic; this results in a nine nodes quadrangular (Q9) DLFE. The latter is validated in free-vibrations, first numerically against ANSYS® three-dimensional piezoelectric finite elements for a cantilever moderately thick aluminum plate with two co-localized piezoceramic patches, and then experimentally against a free quasi-isotropic transverse composite thin plate with four piezoceramic patches. The obtained short-circuit and open-circuit (OC) frequencies were satisfactory for both benchmarks, while the post-treated modal effective electromechanical coupling coefficients agreed well with ANSYS® results (first benchmark) but only fairly with the experimental ones (second benchmark). Once validated, the Q9-DLFE was used to assess numerically the equipotential (EP) physical condition influence on the OC sensed electric potential; for this purpose, the above first benchmark, but with the top piezoceramic patch only, was finally analyzed. It was found that the EP condition homogenizes and lowers the sensed potential on the OC electrode.

Keywords: Discrete layer, finite element, piezoelectric, composite, plate, free-vibration, short-circuit, open-circuit, effective electromechanical coupling coefficient, sensing.

[1] Kuwait University, Mechanical Engineering Department, P.O. Box 5969, Safat 13060, Kuwait.
[2] Institut Supérieur de Mécanique de Paris, Structures, 3 rue Fernand Hainault, 93407 Saint-Ouen CEDEX, France. Corresponding author: benjeddou@supmeca.fr.

1 Introduction

For about four decades now, finite element (FE) models for piezoelectric structures have been continuously developed for all types of structural elements [Benjeddou (2000)]. In the particular case of *composite* structures, the available FEs can be classified into *equivalent single layer* models, that assume a single displacement field through their thickness, or *layer-wise* ones, that assume a different displacement field through the thickness of each layer of the composite. The retained generalized displacements of the last composite FEs category are usually those associated with the mid-layer reference surface. However, to simplify the continuity conditions application, the lay-up FE assembly procedure, and the piezoelectric plies surface electric potentials and charges handling, it is more suitable to retain the variables associated to the layers top and bottom surfaces as unknowns. This leads to the so-called *discrete-layer* FE (DLFE) models. The latter were already developed for sandwich beams with surface-bonded and embedded piezoelectric patches [Benjeddou, Trindade and Ohayon (1997)], for laminated beams with viscoelastic damping layers [Zapfe and Lesieutre (1999)], and recently for laminated composite beams with surface-bonded piezoelectric patches [Al-Ajmi and Benjeddou (2008)]; other than one-dimensional (1D) DLFE, as the geometrically exact piezoelectric solid-shell FE from [Kulikov and Plotnikova (2008)], are rarely available.

The piezoelectric laminated beam 1D DLFE model, recently developed by the authors [Al-Ajmi and Benjeddou (2008)], is naturally extended in this paper to two-dimensional (2D) plate structures. The present plate DLFE, as for the previous beam one, satisfies automatically the *equipotential* (EP) electrode physical condition which is usually ignored in most of piezoelectric FE models as reviewed in [Chevallier, Ghorbel and Benjeddou (2008)]. Hence, in the following, the discrete-layer theoretical formulation is first described; then, the corresponding FE formulation is presented; next, the resulting new DLFE is validated first *numerically* against ANSYS® three-dimensional (3D) FE modal analyses of a *cantilever* isotropic aluminum plate with two co-localized piezoceramic patches under short-circuit (SC) and open-circuit (OC) electric conditions; this serves to evaluate the effective electromechanical coupling coefficient (EMCC) in order to assess the present DLFE electromechanical coupling representation. The new DLFE is then *experimentally* validated against modal analysis tests of a *free* laminated composite plate with four piezoceramic patches under SC and OC electric conditions [Araujo et al (2009)]; the EMCC is also post-treated for the same purpose as above. Once validated, the DLFE is used to assess numerically the EP condition influence on the sensed electric potential; for this purpose the above first benchmark, but with the top piezoceramic patch only, is finally analyzed.

2 Theoretical formulation

This section describes the plate kinematics (discrete-layer displacements and strains), coupled piezoelectric and elastic plane-stress reduced constitutive equations, and Hamilton's principle-based variational equations which are used in the subsequent section for the finite element formulation and derivation of the electromechanically coupled discretized equations of motion.

2.1 Discrete-layer kinematics

The retained kinematics can be classified as a layer-wise first-order shear deformation one in the sense that it assumes that each layer (ply) of the laminated composite plate can be *moderately thick* and deforms under a *plane-stress* state with in-plane displacements, u_1 and u_2, varying *linearly* through each ply thickness z (or 3), and all points through the cross-section of the layer, hence the plate, are assumed to have the *same* transverse deflection, u_3. In addition, perfect bonding is assumed between the composite plate layers, and the patches bonding layers thickness and influence are considered negligible.

The discrete-layer displacement field is then defined for the k^{th} layer as

$$\begin{aligned} u_1(x,y,z) &= F^{k-1}(z)\, u^{k-1}(x,y) + F^{k}(z)\, u^{k}(x,y) \\ u_2(x,y,z) &= F^{k-1}(z)\, \upsilon^{k-1}(x,y) + F^{k}(z)\, \upsilon^{k}(x,y) \\ u_3(x,y,z) &= w(x,y) \end{aligned} \tag{1}$$

Where,

$$x \in [0,a], \quad y \in [0,b], \quad z \in \left[h^k, h^{k-1}\right],$$

$$F^{k-1}(z) = \frac{h^{k-1}-z}{h}, \quad F^{k}(z) = \frac{z-h^k}{h}, \quad h = h^{k-1} - h^k$$

In Equation (1), u^i and υ^i (i = k-1, k) are the in-plane displacements of the k^{th} layer's top and bottom surfaces in x (or 1) and y (or 2) directions, respectively.

The resulting strains are those listed in the following in-plane $\{\varepsilon\}$ and transverse shear $\{\gamma\}$ strain vectors

$$\{\varepsilon\} = \begin{Bmatrix} \varepsilon_1 \\ \varepsilon_2 \\ \varepsilon_6 \end{Bmatrix} = \begin{Bmatrix} u_{1,x} \\ u_{2,y} \\ u_{1,y} + u_{2,x} \end{Bmatrix}, \quad \{\gamma\} = \begin{Bmatrix} \varepsilon_4 \\ \varepsilon_5 \end{Bmatrix} = \begin{Bmatrix} u_{2,z} + u_{3,y} \\ u_{1,z} + u_{3,x} \end{Bmatrix} \tag{2}$$

Where ',' denotes a spatial partial derivation with respect to the variable that follows it.

2.2 Plane-stress reduced constitutive equations

The 3D linear constitutive equations for a piezoelectric material, *poled along its thickness* and in the stress-charge *e-form*, couples the Cauchy stresses σ_p, linearized strains ε_p, electric fields E_k, and electric displacements D_k (p= 1, …, 6; k = 1, 2, 3) as follows

$$\begin{Bmatrix}\sigma_1\\ \sigma_2\\ \sigma_3\\ \sigma_4\\ \sigma_5\\ \sigma_6\\ D_1\\ D_2\\ D_3\end{Bmatrix} = \begin{bmatrix} C_{11}^E & C_{12}^E & C_{13}^E & 0 & 0 & 0 & 0 & 0 & -e_{31}\\ C_{12}^E & C_{22}^E & C_{23}^E & 0 & 0 & 0 & 0 & 0 & -e_{32}\\ C_{13}^E & C_{23}^E & C_{33}^E & 0 & 0 & 0 & 0 & 0 & -e_{33}\\ 0 & 0 & 0 & C_{44}^E & 0 & 0 & 0 & -e_{24} & 0\\ 0 & 0 & 0 & 0 & C_{55}^E & 0 & -e_{15} & 0 & 0\\ 0 & 0 & 0 & 0 & 0 & C_{66}^E & 0 & 0 & 0\\ 0 & 0 & 0 & 0 & e_{15} & 0 & \in_{11}^{\varepsilon} & 0 & 0\\ 0 & 0 & 0 & e_{24} & 0 & 0 & 0 & \in_{22}^{\varepsilon} & 0\\ e_{31} & e_{32} & e_{33} & 0 & 0 & 0 & 0 & 0 & \in_{33}^{\varepsilon}\end{bmatrix} \begin{Bmatrix}\varepsilon_1\\ \varepsilon_2\\ \varepsilon_3\\ \varepsilon_4\\ \varepsilon_5\\ \varepsilon_6\\ E_1\\ E_2\\ E_3\end{Bmatrix} \tag{3}$$

Where, C_{pq}^E, $e_{ip}, \in_{ii}^{\varepsilon}$ (p, q= 1, …, 6; i= 1, 2, 3) are the *shorted* elastic (N/m^2), stress piezoelectric (C/m^2), and *blocked* dielectric (F/m) constants.

Due to the retained *plane-stress* ($\sigma_3 = 0$) and *unidirectional* electric field ($E_x = E_y = 0$) and displacement ($D_x = D_y = 0$) assumptions, the former 3D piezoelectric constitutive equations reduce to the following ones

$$\begin{Bmatrix}\sigma_1\\ \sigma_2\\ \sigma_6\end{Bmatrix} = \begin{bmatrix}\bar{Q}_{11} & \bar{Q}_{12} & 0\\ \bar{Q}_{12} & \bar{Q}_{22} & 0\\ 0 & 0 & \bar{Q}_{66}\end{bmatrix}^E \begin{Bmatrix}\varepsilon_1\\ \varepsilon_2\\ \varepsilon_6\end{Bmatrix} - \begin{Bmatrix}\bar{e}_{31}\\ \bar{e}_{32}\\ 0\end{Bmatrix} E_3, \quad \begin{Bmatrix}\sigma_4\\ \sigma_5\end{Bmatrix} = \begin{bmatrix}\bar{Q}_{44} & 0\\ 0 & \bar{Q}_{55}\end{bmatrix}^E \begin{Bmatrix}\varepsilon_4\\ \varepsilon_5\end{Bmatrix} \tag{4}$$

$$D_3 = \begin{Bmatrix}\bar{e}_{31} & \bar{e}_{32} & 0\end{Bmatrix} \begin{Bmatrix}\varepsilon_1\\ \varepsilon_2\\ \varepsilon_6\end{Bmatrix} + \bar{\in}_{33}^{\varepsilon} E_3$$

Where, for α, β = 1, 2 and m = 4, 5, 6, the plane stress-reduced constants are given by

$$\bar{Q}_{\alpha\beta}^E = C_{\alpha\beta}^E - \frac{C_{\alpha 3}^E C_{\beta 3}^E}{C_{33}^E}, \quad \bar{Q}_{mm}^E = C_{mm}^E; \quad \bar{e}_{3\alpha} = e_{3\alpha} - \frac{C_{\alpha 3}^E}{C_{33}^E} e_{33}, \quad \bar{\in}_{33}^{\varepsilon} = \in_{33}^{\varepsilon} + \frac{e_{33}^2}{C_{33}^E}$$

Equations (4) can be rewritten, respectively, in the following condensed form

$$\{\sigma\} = \left[\bar{Q}^E\right]\{\varepsilon\} - \langle\bar{e}\rangle^T E_3, \quad \{\tau\} = \left[\bar{Q}_s^E\right]\{\gamma\}, D_3 = \langle\bar{e}\rangle\{\varepsilon\} + \bar{\in}_{33}^{\varepsilon} E_3 \tag{5}$$

Where, the subscript *s* denotes *shear*, and the transverse electric field was assumed *constant* through the ply thickness so that it reads

$$E_3 = -\frac{V}{h} \tag{6}$$

With, $V = \phi^{k-1} - \phi^k$ denoting the electric potential difference between the upper and lower equipotential electrodes of the piezoelectric ply of thickness h, respectively.

The in-plane and shear coefficients of the elastic matrices of equation (5) can be defined in terms of the engineering constants (Young's moduli E_α, shear moduli G_{12} and $G_{\alpha 3}$ and Poisson's ratios ν_{12} and ν_{21}), for *orthotropic* composite and piezoelectric plies, by

$$\bar{Q}_{11} = \frac{E_1}{1-\nu_{12}\nu_{21}}, \quad \bar{Q}_{12} = \frac{\nu_{12}E_2}{1-\nu_{12}\nu_{21}}, \quad \bar{Q}_{22} = \frac{E_2}{1-\nu_{12}\nu_{21}}, \tag{7}$$

$$\bar{Q}_{66} = G_{12}, \quad \bar{Q}_{44} = G_{23}, \quad \bar{Q}_{55} = G_{13}$$

For an angle-ply composite layer, the transformed elastic constitutive equations become

$$\{\sigma\} = [Q]\{\varepsilon\}, \quad \{\tau\} = [Q_s]\{\gamma\} \tag{8}$$

With,

$$[Q] = \begin{bmatrix} Q_{11} & Q_{12} & Q_{16} \\ Q_{12} & Q_{22} & Q_{26} \\ Q_{16} & Q_{26} & Q_{66} \end{bmatrix}, \quad [Q_s] = \begin{bmatrix} Q_{44} & Q_{45} \\ Q_{45} & Q_{55} \end{bmatrix}$$

Where, the Q_{pq} expressions are given in the Appendix.

2.3 Coupled variational formulation

The variational formulation uses this piezoelectric-extended Hamilton's principle,

$$\int_{t_1}^{t_2} (\delta T - \delta H + \delta W)\, dt = 0 \tag{9}$$

Where, δH is the piezoelectric ply virtual electromechanical enthalpy which reduces to

$$\delta H = \int_\Omega \left(\{\delta\varepsilon\}^T \{\sigma\} + \{\delta\gamma\}^T \{\tau\} - \delta E_3\, D_3 \right) d\Omega \tag{10}$$

δT is the ply (of mass densityρ) virtual kinetic energy given by ('˙' = time derivation)

$$\delta T = \int_{\Omega} (\delta \dot{u}_1 \, \dot{u}_1 + \delta \dot{u}_2 \, \dot{u}_2 + \delta \dot{u}_3 \, \dot{u}_3) \, \rho d\Omega \tag{11}$$

δW is the external virtual work that is here considered due to only the applied mechanical (m) transverse force F_z on the surface S_F and the electric (e) surface charge Q_e on the surface S_Q; it is then defined by

$$\delta W = \delta W_m + \delta W_e = \int_{S_F} \delta w \, F_z \, dS_F - \int_{S_Q} \delta \phi \, Q_e \, dS_Q \tag{12}$$

3 Finite element formulation

This section describes the generalized displacements in-plane interpolations and resulting strains and transverse electric field discretizations that should be substituted in above variational equation (9) in order to get the *discretized equations of motion*; then, focus is made on deriving the *free-vibration problems*, under SC and OC electric boundary conditions, from which the effective modal EMCC is post-processed. OC and SC *static sensing problems* are finally derived in order to assess the EP physical condition influence on the computed electric potential of the sensor electrode.

3.1 Discretized equations of motion

Each layer of the FE has *corner nodal in-plane displacements* degrees of freedom (DOF), as in Fig. 1a, and all layers, forming an element in thickness direction, have the *same nodal transverse displacements* DOF (Fig. 1b); the k^{th} ply DOF vector is then defined by

$$\{q\} = \{Y_1, W_1, W_2, Y_2, W_3, W_4, Y_3, W_5, W_6, Y_4, W_7, W_8, W_9\} \tag{13}$$

With,

$$\{Y_i\} = \left\{ U_i^{k-1}, U_i^k, V_i^{k-1}, V_i^k \right\} \; ; \; i = 1, ..., 4$$

The discretized surface in-plane and transverse displacements are then given by

$$u^j = \left\{ N_u^j \right\} \{q\}, \quad \upsilon^j = \left\{ N_\upsilon^j \right\} \{q\}; \quad (j = k-1, k); \quad w = \{N_w\} \{q\} \tag{14}$$

Where, N_u^j, N_υ^j and N_w are *bilinear* in-plane and *bi-quadratic* transverse shape functions.

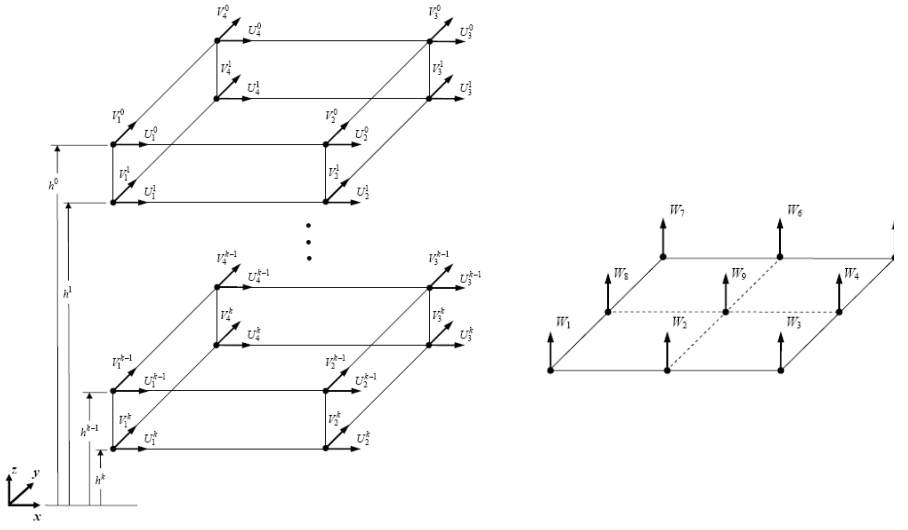

(a) Discrete-layer in-plane nodal displacements (b) Plate nodal transverse deflections

Figure 1: Discrete-layer in-plane nodal displacements (a) and plate nodal deflections (b).

The discretized in-plane displacements then become

$$u_1 = \{N_u\}\{q\}, \quad u_2 = \{N_\upsilon\}\{q\} \tag{15}$$

Where,

$$\{N_u\} = F^{k-1}\left\{N_u^{k-1}\right\} + F^k\left\{N_u^k\right\}, \quad \{N_\upsilon\} = F^{k-1}\left\{N_\upsilon^{k-1}\right\} + F^k\left\{N_\upsilon^k\right\}$$

Then, substituting equation (15) in equations (1, 2) gives these discretized strain vectors

$$\{\varepsilon\} = [B]\{q\}, \quad \{\gamma\} = [B_s]\{q\} \tag{16}$$

With

$$[B] = \begin{bmatrix} F^{k-1}\frac{\partial}{\partial x}\left\{N_u^{k-1}\right\} + F^k\frac{\partial}{\partial x}\left\{N_u^k\right\} \\ F^{k-1}\frac{\partial}{\partial x}\left\{N_\upsilon^{k-1}\right\} + F^k\frac{\partial}{\partial x}\left\{N_\upsilon^k\right\} \\ F^{k-1}\left\{\frac{\partial}{\partial x}\left\{N_\upsilon^{k-1}\right\} + \frac{\partial}{\partial y}\left\{N_u^{k-1}\right\}\right\} + F^k\left\{\frac{\partial}{\partial x}\left\{N_\upsilon^k\right\} + \frac{\partial}{\partial y}\left\{N_u^k\right\}\right\} \end{bmatrix}$$

$$[B_s] = \begin{Bmatrix} \frac{1}{h}\left(\{N_u^{k-1}\} - \{N_u^k\}\right) + \frac{\partial}{\partial x}\{N_w\} \\ \frac{1}{h}\left(\{N_\upsilon^{k-1}\} - \{N_\upsilon^k\}\right) + \frac{\partial}{\partial y}\{N_w\} \end{Bmatrix}$$

The electric field, given in equation (6), is in fact self-discretized and can be re-written as

$$E_3 = \begin{Bmatrix} -\frac{1}{h} & \frac{1}{h} \end{Bmatrix}^T \begin{Bmatrix} \phi^{k-1} \\ \phi^k \end{Bmatrix} = \{N_\phi\}^T \{\phi\} \tag{17}$$

Finally, substituting the discretized strains (16) and the electric field (17) in the variational equations (9) - (12), provides the following ply coupled equations of motion

$$\begin{bmatrix} [K_{mm}] & [K_{me}] \\ [K_{me}]^T & -[K_{ee}] \end{bmatrix} \begin{Bmatrix} \{q\} \\ \{\phi\} \end{Bmatrix} + \begin{bmatrix} [M_{mm}] & [0] \\ [0]^T & [0] \end{bmatrix} \begin{Bmatrix} \{\ddot{q}\} \\ \{\ddot{\phi}\} \end{Bmatrix} = \begin{Bmatrix} \{F\} \\ -\{Q_e\} \end{Bmatrix} \tag{18}$$

With,

$$[M_{mm}] = \int_0^a \int_0^b \int_{h_k}^{h_{k-1}} \left(\{N_u\}^T \{N_u\} + \{N_\upsilon\}^T \{N_\upsilon\} + \{N_w\}^T \{N_w\} \right) \rho \, dz \, dy \, dx$$

$$[K_{mm}] = \int_0^a \int_0^b \int_{h_k}^{h_{k-1}} \left([B]^T [Q] [B] + [B_s]^T [Q_s] [B_s] \right) dz \, dy \, dx$$

$$[K_{me}] = -\int_0^a \int_0^b \int_{h_k}^{h_{k-1}} \left([B]^T \{\bar{e}\}^T \{N_\phi\} \right) dz \, dy \, dx$$

$$[K_{ee}] = -\int_0^a \int_0^b \int_{h_k}^{h_{k-1}} \left(\{N_\phi\}^T \bar{\in}_{33}^{\varepsilon} \{N_\phi\} \right) dz \, dy \, dx$$

$$\{F\} = \int_{S_F} \{N_w\}^T F_z \, dS_F$$

In addition, $\{Q_e\}$ is a vector of electric charges on the electrodes' surfaces resulting from the second part of equation (12) which can be re-written as

$$\delta W_\phi = -\{\delta\phi\}^{\mathrm{T}} \{Q_e\}, \quad \{Q_e\} = \begin{Bmatrix} Q_e^{k-1} \\ -Q_e^k \end{Bmatrix} \tag{19}$$

Where, Q_e^{k-1} and Q_e^k are the electric surface charges on the piezoelectric ply upper and lower electrodes, respectively.

The elastic plies are assembled in the thickness direction to form a composite element and then the assembly process proceeds to the surface area. The piezoelectric plies, if they exist, are assembled after the global assembly of the composite plate

such that the global DOF vector is made of the mechanical DOF of the composite plate, $\{\mathbf{q}\}$, followed by that of the piezoelectric layer one, $\{\varphi\}$.

The assembled equations of motion can be written now in this global form

$$\begin{bmatrix} [\mathbf{K}_{mm}] & [\mathbf{K}_{me}] \\ [\mathbf{K}_{me}]^T & -[\mathbf{K}_{ee}] \end{bmatrix} \begin{Bmatrix} \{\mathbf{q}\} \\ \{\phi\} \end{Bmatrix} + \begin{bmatrix} [\mathbf{M}] & [\mathbf{0}] \\ [\mathbf{0}]^T & [\mathbf{0}] \end{bmatrix} \begin{Bmatrix} \{\ddot{\mathbf{q}}\} \\ \{\ddot{\phi}\} \end{Bmatrix} = \begin{Bmatrix} \{\mathbf{F}\} \\ -\{\mathbf{Q}\} \end{Bmatrix} \tag{20}$$

Where, $\{\mathbf{q}\}$, $\{\varphi\}$, $\{\mathbf{F}\}$ and $\{\mathbf{Q}\}$ are global vectors of those previously defined.

To form *equipotential* electrodes, all piezoelectric elements that form a continuous surface of an electrode (meshed with m FEs) must have the *same* surface potential so that

$$\phi_1^{k-1} = \phi_2^{k-1} = \cdots = \phi_m^{k-1}, \quad \phi_1^k = \phi_2^k = \cdots = \phi_m^k \tag{21}$$

Therefore, the global electric DOFs vector is redefined as

$$\{\phi\} = [\mathbf{P}]\{\mathbf{v}\} \tag{22}$$

Where, $[\mathbf{P}]$ is a Boolean matrix and $\{\mathbf{v}\}$ denotes the vector of *electrodes potentials*.

Applying the last relationship to the global equation of motion (20) results in these transformed ones

$$\begin{bmatrix} [\mathbf{K}_{mm}] & [\bar{\mathbf{K}}_{me}] \\ [\bar{\mathbf{K}}_{me}]^T & -[\bar{\mathbf{K}}_{ee}] \end{bmatrix} \begin{Bmatrix} \{\mathbf{q}\} \\ \{\mathbf{v}\} \end{Bmatrix} + \begin{bmatrix} [\mathbf{M}] & [\mathbf{0}] \\ [\mathbf{0}]^T & [\mathbf{0}] \end{bmatrix} \begin{Bmatrix} \{\ddot{\mathbf{q}}\} \\ \{\ddot{\mathbf{v}}\} \end{Bmatrix} = \begin{Bmatrix} \{\mathbf{F}\} \\ -\{\bar{\mathbf{Q}}\} \end{Bmatrix} \tag{23}$$

Where,

$$[\bar{\mathbf{K}}_{me}] = [\mathbf{K}_{me}][\mathbf{P}], \quad [\bar{\mathbf{K}}_{ee}] = [\mathbf{P}]^T [\mathbf{K}_{ee}][\mathbf{P}], \quad \{\bar{\mathbf{Q}}\} = [\mathbf{P}]^T \{\mathbf{Q}\}$$

3.2 Free-vibration problems

Two free-vibration problems can be formulated for OC and SC electric boundary conditions. The OC analysis requires the piezoelectric surfaces to be charge free; hence, the global electric charge vector vanishes, leading to this OC harmonic free-vibration problem

$$\left(\begin{bmatrix} [\mathbf{K}_{mm}] & [\bar{\mathbf{K}}_{me}] \\ [\bar{\mathbf{K}}_{me}]^T & -[\bar{\mathbf{K}}_{ee}] \end{bmatrix} - \omega^2 \begin{bmatrix} [\mathbf{M}] & [\mathbf{0}] \\ [\mathbf{0}]^T & [\mathbf{0}] \end{bmatrix} \right) \begin{Bmatrix} \{\mathbf{q}\} \\ \{\mathbf{v}\} \end{Bmatrix} = \begin{Bmatrix} \{\mathbf{0}\} \\ \{\mathbf{0}\} \end{Bmatrix} \tag{24}$$

Static condensation of electrodes voltage DOFs reduces the last system to this one

$$\left([\mathbf{K}^{oc}] - \omega^2[\mathbf{M}]\right)\{\mathbf{q}\} = \{0\} \tag{25}$$

With,

$$[\mathbf{K}^{oc}] = [\mathbf{K}_{mm}] + \left[\bar{\mathbf{K}}_{me}\right]\left[\bar{\mathbf{K}}_{ee}\right]^{-1}\left[\bar{\mathbf{K}}_{me}\right]^{T}$$

Solving the equation (25) leads, in particular, to the OC natural frequencies (Hz), f_{oc}.

Under SC electric conditions, the electrodes electric potential DOFs vector is nil and the harmonic free-vibration problem, resulting from equation (23), is now purely mechanical

$$\left([\mathbf{K}_{mm}] - \omega^2[\mathbf{M}]\right)\{\mathbf{q}\} = \{0\} \tag{26}$$

Solving equation (26) provides, in particular, the SC natural frequencies (Hz), f_{sc}.

From OC and SC natural frequencies, the squared modal effective EMCC is defined as

$$K^2 = \frac{f_{oc}^2 - f_{sc}^2}{f_{sc}^2} \tag{27}$$

The EMCC is an indicator of the electromechanical coupling representation; in particular, it shows which mode is electromechanically coupled or not; hence, it can be used as a pre-design tool for several applications such as piezoceramic shunted damping (Chevallier, Ghorbel and Benjeddou (2009)], sensors/actuators positions optimization [Trindade and Benjeddou (2009)], or damage detection [Al-Ajmi and Benjeddou (2008)].

3.3 Static sensing problems

The sensed voltage can be measured under an applied mechanical load. As for the free vibrations, there are two sensing problems depending on the considered electric conditions (SC or OC) for the sensors electrodes. In order to assess the EP physical condition influence on the computed sensed voltage, sensing problems are derived, in the following, for the two cases: without and with EP constraints.

The static OC sensing analysis requires the piezoelectric surfaces to be charge free; hence, when the EP conditions (21, 22) are not enforced, the global electric charge vector vanishes in equation (20), leading to this static OC sensing coupled problem

$$\begin{bmatrix} [\mathbf{K}_{mm}] & [\mathbf{K}_{me}] \\ [\mathbf{K}_{me}]^T & -[\mathbf{K}_{ee}] \end{bmatrix} \begin{Bmatrix} \{\mathbf{q}\} \\ \{\phi\} \end{Bmatrix} = \begin{Bmatrix} \{\mathbf{F}\} \\ \{\mathbf{0}\} \end{Bmatrix} \tag{28}$$

From the second line of the last equation, the OC sensing potentials can be deduced as

$$\{\phi\} = [\mathbf{K}_{ee}]^{-1}[\mathbf{K}_{me}]^T\{\mathbf{q}\} \tag{29}$$

Where, $\{\mathbf{q}\}$ is the solution of this potentials-condensed static mechanical problem (after substituting equation (29) in the first line of equation (28))

$$([\mathbf{K}_{mm}] + [\mathbf{K}_{me}] [\mathbf{K}_{ee}]^{-1} [\mathbf{K}_{me}]^T) \{\mathbf{q}\} = \{\mathbf{F}\} \tag{30}$$

When the EP conditions (21, 22) are enforced, equation (23) provides the following static OC sensing coupled problem

$$\begin{bmatrix} [\mathbf{K}_{mm}] & [\bar{\mathbf{K}}_{me}] \\ [\bar{\mathbf{K}}_{me}]^T & -[\bar{\mathbf{K}}_{ee}] \end{bmatrix} \begin{Bmatrix} \{\mathbf{q}\} \\ \{\mathbf{v}\} \end{Bmatrix} = \begin{Bmatrix} \{\mathbf{F}\} \\ \{\mathbf{0}\} \end{Bmatrix} \tag{31}$$

EP-enforced sensing voltages can then be obtained analogically to equation (29) as

$$\{\mathbf{v}\} = [\bar{\mathbf{K}}_{ee}]^{-1} [\bar{\mathbf{K}}_{me}]^T \{\mathbf{q}\} \tag{32}$$

Where, $\{\mathbf{q}\}$ is the solution of this potentials-condensed static mechanical problem (after substituting back equation (32) into equation (31))

$$([\mathbf{K}_{mm}] + [\bar{\mathbf{K}}_{me}] [\bar{\mathbf{K}}_{ee}]^{-1} [\bar{\mathbf{K}}_{me}]^T) \{\mathbf{q}\} = \{\mathbf{F}\} \tag{33}$$

Under SC electric conditions and when the EP conditions (21, 22) are not enforced in equation (20), the electrodes electric potential DOFs vector vanishes in the latter equation leading to the following static SC sensing problem

$$\begin{bmatrix} [\mathbf{K}_{mm}] & [\mathbf{K}_{me}] \\ [\mathbf{K}_{me}]^T & -[\mathbf{K}_{ee}] \end{bmatrix} \begin{Bmatrix} \{\mathbf{q}\} \\ \{\mathbf{0}\} \end{Bmatrix} = \begin{Bmatrix} \{\mathbf{F}\} \\ -\{\mathbf{Q}\} \end{Bmatrix} \tag{34}$$

From the second line of the last equation, the SC sensing charges can be deduced as

$$\{\mathbf{Q}\} = -[\mathbf{K}_{me}]^T \{\mathbf{q}\} \tag{35}$$

Where, $\{\mathbf{q}\}$ is the solution of this mechanical static problem (from first line of (34))

$$[\mathbf{K}_{mm}] \{\mathbf{q}\} = \{\mathbf{F}\} \tag{36}$$

When the EP conditions (21, 22) are enforced in equation (20), equation (23) provides the following static OC sensing coupled problem

$$\begin{bmatrix} [\mathbf{K}_{mm}] & [\bar{\mathbf{K}}_{me}] \\ [\bar{\mathbf{K}}_{me}]^T & -[\bar{\mathbf{K}}_{ee}] \end{bmatrix} \begin{Bmatrix} \{\mathbf{q}\} \\ \{\mathbf{0}\} \end{Bmatrix} = \begin{Bmatrix} \{\mathbf{F}\} \\ -\{\bar{\mathbf{Q}}\} \end{Bmatrix} \tag{37}$$

EP-enforced sensing voltages can then be obtained from the last equation's second line as

$$\{\bar{\mathbf{Q}}\} = -\left[\overline{\mathbf{K}}_{me}\right]^T \{\mathbf{q}\} \tag{38}$$

Where, $\{\mathbf{q}\}$ is the solution of this static mechanical problem (from first line of (37))

$$[\mathbf{K}_{mm}]\{\mathbf{q}\} = \{\mathbf{F}\} \tag{39}$$

The comparison of equations (32,33) to equations (38,39) indicates that the EP condition is expected to be more influential for the computed OC sensing voltage, equation (32), than for the SC sensing charge, equation (38); this is due to the fact that the mechanical static problem resulting from the SC electric condition, as shown by equations (36) and (39), is unchanged by the EP condition, while the corresponding one, as shown by equations (30) and (33), for the OC condition is modified by the EP condition. Hence, in the validation section, the EP physical condition influence is assessed only for the computed OC sensing voltages.

4 Free-vibrations validation and static OC sensing analysis

The piezoelectric adaptive composite plate Q9-DLFE is hereafter validated first numerically against ANSYS® (version 10) 3D FE modal analyses of a cantilever isotropic aluminum plate with co-localized piezoceramic patches (PIC255 from PI Germany) under SC and OC electric conditions in order to assess the electromechanical coupling representation of the present DLFE through the EMCC evaluation; then, the Q9-DLFE is experimentally and numerically validated via modal analyses of a free laminated composite plate with four PIC255 piezoceramic patches under SC and OC electric conditions; the EMCC is also post-treated for the same purpose as above. Once validated, the Q9-DLFE is used to assess numerically the EP physical condition influence on the computed OC sensing voltage; for this purpose, the above first benchmark, but with the top piezoceramic patch only, is finally analyzed.

4.1 Cantilever isotropic plate with a pair of co-localized piezoceramic patches

The benchmark proposed by [Chevallier, Ghorbel, and Benjeddou (2008)] is here first considered; it consists of a cantilever moderately thick aluminum plate with a pair of symmetrically bonded piezoceramic PIC255 patches as shown in Fig. 2.

The base isotropic plate has a thickness of h = 3.9 mm, Young's modulus of E= 69 GPa, mass density of $\rho = 2790$ kg/m^3 and Poisson's ratio of ν= 0.3. Each PIC255 piezoceramic patch has a thickness of 0.3 mm. The plate is 79 mm long and the

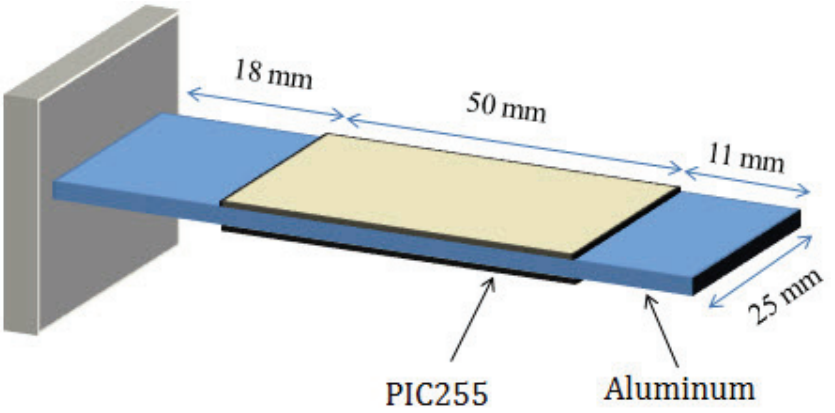

Figure 2: Cantilever aluminum plate with co-localized PIC255 patches

50 mm long patches pair is placed 18 mm from the fixed end. Both of the base plate and the patches have a common width of 25 mm. The PIC255 patches electromechanical isotropic-transverse plane stress-reduced properties are: $\bar{Q}^E_{11} = \bar{Q}^E_{22}$= 69.18 GPa, $\bar{Q}^E_{12}$= 22.14 GPa, $\bar{Q}^E_{44} = \bar{Q}^E_{55}$= 21 GPa, $\bar{Q}^E_{66}$= 23.5 GPa, mass density ρ= 7720 Kg/m^3, $\bar{e}_{31} = \bar{e}_{32}$= -16.57 C/m^2 and $\bar{\in}^{\varepsilon}_{33}$= 9.52 nF/m. The corresponding full 3D properties are given in [Chevallier, Ghorbel and Benjeddou (2008, 2009)]. The DLFE model is made of two elastic plies for the aluminum base structure in addition to the upper and lower piezoelectric plies, and meshed with 8 elements in the width and 38 elements in the length (8 elements from the fixed end to the piezoceramic patch, 25 elements for the piezoceramic section, and 5 elements for the free end section) leading to a 304 FE model.

The modal effective squared EMCC (%) results are post-processed from the SC and OC natural frequencies (Hz) resulting from the present piezoelectric plate Q9-DLFE, and compared to those from piezoelectric 3D FE analyses with ANSYS®. As can be seen in Tab. 1, the present Q9-DLFE predictions, for both calculated SC and OC frequencies (Hz) and post-treated squared EMCC (%) values of the first four modes, are in good agreement with the reference [Chevallier, Ghorbel and Benjeddou (2008)] results obtained using ANSYS® full quadratic (20 nodes) 3D FE simulations (1700 FE model).

4.2 Free laminated composite plate with four piezoceramic patches

The second validation example is taken from [Araujo, Mota Soares, Friedmann, Röhner, Henkel (2009)]; it is a free composite plate of aeronautic type that is

Table 1: ANSYS® quadratic 3D FE [Chevallier, Ghorbel and Benjeddou (2008)] vs. present plate Q9-DLFE results for the aluminum adaptive cantilever plate.

Mode	$f_{oc}(Hz)$			$f_{sc}(Hz)$			K^2 (%)		
	3D	DLFE	Er* (%)	3D	DLFE	Er* (%)	3D	DLFE	Er* (%)
1	495.61	495.46	-0.03	493.07	492.87	-0.04	1.03	1.05	1.94
2	2797.9	2808.2	0.37	2797.9	2808.2	0.37	0	0	0
3	3044.1	3099.4	1.82	3044.1	3099.4	1.82	0	0	0
4	3317.7	3322.5	0.14	3249.0	3251.7	0.08	4.27	4.40	3.04

* Er (%) = 100 (DLFE-3D)/3D

made of 16 plies in a symmetric stacking sequence: [90/45/0/-45/90/45/0/-45/-45/0/45/90/-45/0/45/90]. The total thickness of the whole composite plate is 4.13 mm equally distributed on all plies. Each ply of the composite has the following properties as *identified* by [Araujo, Mota Soares, Friedmann, Röhner, Henkel (2009)] using a *modal – based mixed experimental – plate FE optimization inverse* approach: E_1 = 130.8 GPa, E_2 = 10.6 GPa, G_{12} = 5.6 GPa, G_{13} = 4.2 GPa, G_{23}=3.0 GPa, ν_{12} = 0.36, and ρ = 1543 kg/m^3. Four PIC255 patches, of dimensions 50×50×0.9 mm^3 are bonded to the plate on one side only as in Fig. 3. The properties of the PIC255 in this example are calculated, from those *identified* in [Araujo, Mota Soares, Friedmann, Röhner, Henkel (2009)] with the same above approach, as: $\bar{Q}^E_{11}$= 55.05 GPa, $\bar{Q}^E_{22}$= 49.86 GPa, $\bar{Q}^E_{12}$= 14.46 GPa, $\bar{Q}^E_{44}$= 20.6 GPa, $\bar{Q}^E_{55}$= 8 GPa, $\bar{Q}^E_{66}$= 14.3 GPa, ρ = 7800 kg/m^3, $\bar{e}_{31}$= -17.0 C/m^2, $\bar{e}_{32}$= -12.2 C/m2, $\bar{\in}^{\varepsilon}_{33}$= 9.52 nF/m; notice that the latter value and mass density were not identified in [Araujo, Mota Soares, Friedmann, Röhner, Henkel (2009)].

The Q9-DLFE is here used to compute SC and OC frequencies (Hz) which are post-treated to get the squared EMCC (%); an in-plane 8×12 plate DLFE mesh is considered with 16 plies for the composite plate, and one more ply for the piezoelectric patches. The Q9-DLFE results are compared to the corresponding experimental ones from [Araujo, Mota Soares, Friedmann, Röhner, Henkel (2009)] and presented in Tab. 2. The latter shows that the Q9-DLFE frequency predictions for OC and SC are satisfactory when compared with the experimental results; however, its resulting squared EMCC values mostly differ due to their sensitivity to minimal frequency deviation [Chevallier and Benjeddou (2009)] since they are defined from small differences of squared frequency values.

Table 2 shows that the DLFE 3^{rd}, 5^{th} and 6^{th} modes are electromechanically uncoupled (with zero EMCC), while the tests show them slightly coupled. To check this important difference, the same example has been run using ANSYS® full quadratic

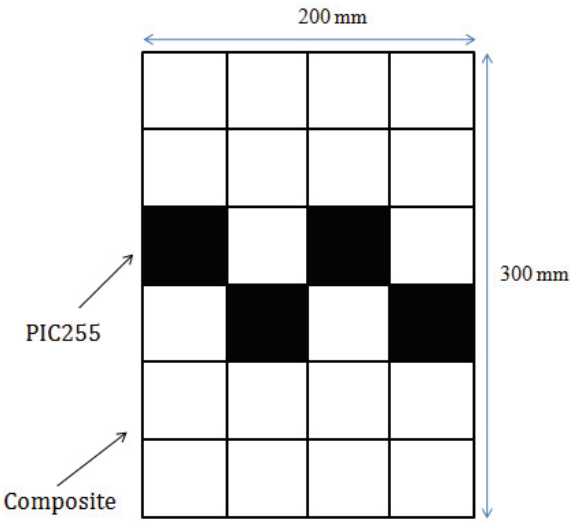

Figure 3: Free composite plate with four PIC255 patches

Table 2: Experimental [Araujo, Mota Soares, Friedmann, Röhner, Henkel (2009)] vs. present 2D DLFE results for the free composite plate with four piezoceramic patches.

Mode	$f_{oc}(Hz)$			$f_{sc}(Hz)$			K^2 (%)		
	Exp.	DLFE	Er* (%)	Exp.	DLFE	Er* (%)	Exp.	DLFE	Er*
1	243.75	240.00	-1.54	243.13	239.77	-1.38	0.51	0.19	-62.74
2	313.75	312.81	-0.30	311.88	311.92	0.01	1.20	0.58	-51.67
3	543.75	551.53	1.43	541.56	551.53	1.84	0.81	0	-
4	576.88	588.67	2.04	571.56	582.44	1.90	1.87	2.15	14.97
5	735.31	738.20	0.39	734.69	738.20	0.48	0.17	0	-
6	878.44	893.14	1.67	874.69	893.14	2.11	0.86	0	-
7	1025.0	1052.1	2.64	1019.1	1051.5	3.18	1.16	0.12	-89.65

* Er (%) = 100 (DLFE-Exp)/Exp

(20 nodes) composite (SOLID191) and piezoelectric (SOLID226) 3D FE model. However since only plane stress - reduced PIC255 data have been identified in [Araujo, Mota Soares, Friedmann, Röhner, Henkel (2009)], the lacking 3D elastic, piezoelectric and dielectric (not identified) data were completed from its manufacturer related data sheet as: E_3 = 47.7 GPa, $\nu_{13} = \nu_{23}$ = 0.44, $e_{31} = e_{32}$ = -7.15 C/m^2, e_{33}= 13.7 C/m^2, e_{15}=e_{24}=11.9 C/m^2, $\in_{11}^{\varepsilon} = \in_{22}^{\varepsilon}$ = 8.234 nF/m, $\in_{33}^{\varepsilon}$ = 7.588 nF/m.

Using these 3D data and equation (4), the plane stress – reduced data used for the DLFE simulations are computed as: $\bar{Q}^E_{11}$= 55.574 GPa, $\bar{Q}^E_{22}$= 53.533 GPa, $\bar{Q}^E_{12}$= 19.65 GPa, $\bar{Q}^E_{44}$= 20.6 GPa, $\bar{Q}^E_{55}$= 8 GPa, $\bar{Q}^E_{66}$= 14.3 GPa, $\rho = 7800$ kg/m^3, $\bar{e}_{31}$= -15.64 C/m^2, $\bar{e}_{32}$= -14.839 C/m2, $\bar{\in}^{\varepsilon}_{33}$= 9.5119 nF/m.

The obtained results, as shown in Table 3, confirm that modes 3, 5 and 6 are uncoupled. Moreover, Table 3 indicates that, with the present data that use the manufacturer piezoelectric coupling and dielectric constants, the DLFE results are now closer to the experimental ones since the computed EMCC for the higher coupled modes 2 and 4, the experimental (1.20 %, 1.87%) and DLFE (1.17%, 1.83%) results are now very close. This indicates that the identified reduced piezoelectric coupling constants are not satisfactory.

Table 3: ANSYS® full quadratic 3D FE vs. present 2D DLFE results for the free composite plate with four piezoceramic patches.

Mode	$f_{oc}(Hz)$			$f_{sc}(Hz)$			K^2 (%)		
	3D	DLFE	Er* (%)	3D	DLFE	Er* (%)	3D	DLFE	Er*
1	243.38	240.05	-1.37	242.87	239.82	-1.26	0.42	0.19	-54.76
2	317.59	313.77	-1.20	311.37	311.95	0.19	4.04	1.17	-71.04
3	538.38	551.99	2.53	538.38	551.99	2.53	0	0	-
4	586.91	588.15	0.21	572.91	582.84	1.73	4.95	1.83	-63.03
5	733.07	738.00	0.67	733.07	738.00	0.67	0	0	-
6	873.87	893.95	2.30	873.87	893.95	2.30	0	0	-
7	1013.6	1053.2	3.91	1013.0	1052.8	3.93	0.12	0.06	-50.00

* Er (%) = 100 (DLFE-3D)/3D

4.3 EP condition effect on the static OC sensed voltage

Physically, the computed potentials on the sensor electrodes should be constant due to the EP condition. However, in the literature, they are often shown continuously (for nodal approximation) or step-wise (for element approximation) linearly decreasing from the cantilever to the free end of the piezoelectric structure. As it was shown above (see sub-section 3.3) theoretically that the computed OC sensed potential is more sensitive to the EP than the SC one, the aim here is to assess the EP physical condition influence only on the computed OC sensing electric potential of the piezoelectric patches electrodes.

To evaluate the effect of the EP electrode physical condition on the OC sensed voltage, the first example of the cantilever plate is considered, but with one piezoceramic patch only attached to the upper surface of the plate as shown in Fig. 4.

By applying a unit transverse load (F=1N) at one of the corner tips of the beam (see Fig. 4), the potential difference vector can be calculated without and with EP condition by equations (29) and (32), respectively. To calculate the potential difference, the electric DOF corresponding to the lower electrode are grounded. This can be done in practice by eliminating the rows and columns corresponding to the grounded electrode (zero potential) from the stiffness matrix. Two plies are used to model the base plate through the thickness and one ply for the piezoelectric patch. The used mesh has 6 FE along width and 15 FE along length (3 FE from fix to patch, 10 for patch, and 2 from patch to free end). Fig. 5a shows the potential difference, without EP condition, while the case with EP is shown in Fig. 5b; both figures represent, as in-plane axes values, the number of piezoelectric elements along the patch width and length.

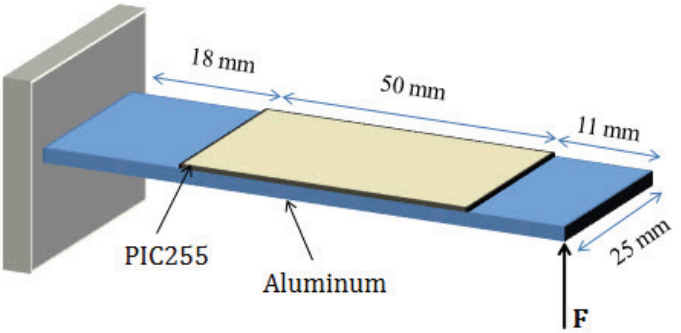

Figure 4: Cantilever aluminum plate with single PIC255 patch

It can be seen from Fig. 5a that the sensed voltage without EP electrode condition makes good physical sense with the piezoelectric patch coupling since each element in this case will virtually has its own set of electrodes. Hence, the sensed voltage is higher from the clamped side due to higher strains and vice versa. However, in practice, a piezoelectric patch usually has one electrode at each of its major surfaces that renders its electric potential spatially uniform. As is shown in Fig. 5b, this has as consequences, not only to homogenize (to make the electric potential spatially uniform) but also to lower the computed sensed voltage; quantitatively, Fig. 5 shows that the uniform voltage obtained after enforcing the EP condition is about 3V under a unit load, and the voltage calculated without enforcing the EP condition varies linearly from about 4V to about 1V. Hence, it can be concluded that, in order to reach accurate computation of the sensing voltages, it is mandatory to apply the EP electrode physical condition.

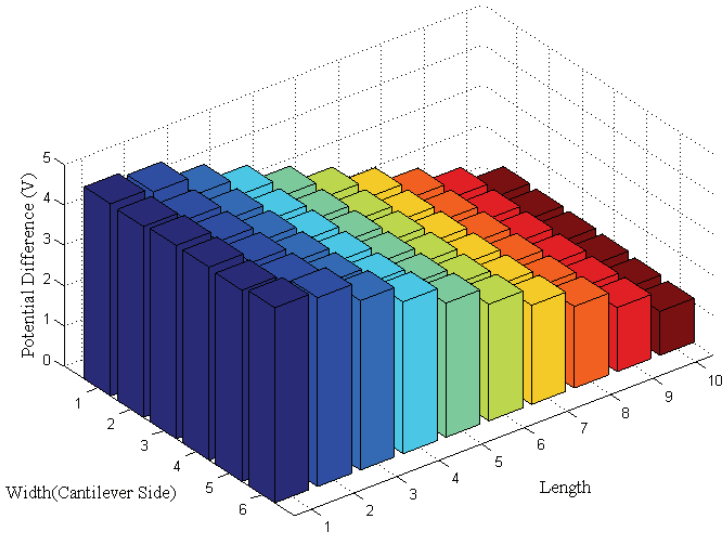

(a)

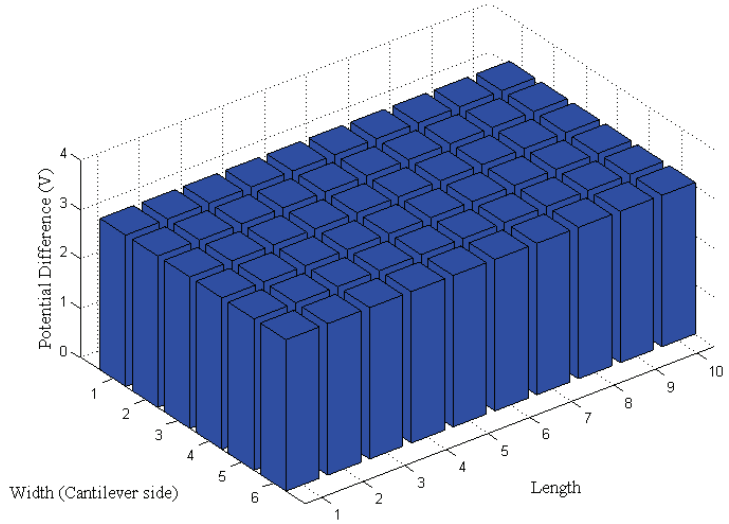

(b)

Figure 5: OC sensed voltage (a) without EP and (b) with EP condition application on the patch electrodes for an applied unit load (F=1N) at the cantilever Al plate corner tip

5 Conclusions and perspectives

A new piezoelectric adaptive plate *discrete-layer* finite element (DLFE) has been formulated on the basis of the first-order shear deformation theory for each ply of the multilayer construction with the top and bottom layer surfaces in-plane displacements and plate transverse deflection as mechanical unknowns; the former were assumed Lagrange linear, while the latter was considered Lagrange quadratic, leading to a *nine-nodes quadrangular* (Q9) DLFE having these mechanical unknowns as *nodal* degrees of freedom (DOF), and the voltage as the *piezoelectric ply* electric DOF. The *equipotential* (EP) physical condition of the piezoelectric layer(s) electrodes was enforced.

This new Q9-DLFE validation on a moderately thick cantilever aluminum rectangular plate with a co-localized piezoceramic large patches pair was satisfactory for both calculated short-circuit (SC) and open-circuit (OC) frequencies and post-treated modal effective electromechanical coupling coefficients (EMCC); however, its validation on a free *quasi-isotropic transverse* composite plate with four piezoceramic patches was satisfactory for the SC and OC frequencies but only fairly for most of the post-treated modal effective EMCCs due to the highly sensitive definition of the latter. Once validated, this new Q9-DLFE was used to assess the EP physical condition influence on the computed OC sensed voltage of a single large patch bonded to the upper surface of the same cantilever aluminum beam of the first benchmark. It was found that, to be accurate in simulating the physics, the EP constraints have to be mandatory enforced on the patch electrodes for both SC and OC sensors. In addition, the numerical analysis has shown that besides making the sensed electric potential uniform, the EP condition lowers the computed sensed voltage compared to that calculated without the EP constraints. Moreover, corresponding theoretical equations showed that the EP constraints should be more influential for the OC, than the SC, electric conditions on the patch electrodes.

As an immediate extension, this Q9-DLFE shall include a quadratic potential approximation as was already made in the corresponding beam one [Al-Ajmi and Benjeddou (2008)] in order to assess its influence on the computed sensed voltage without and with enforcing the EP physical constraints. Then, the beam and plate DLFE formulations and analyses could be extended to the d_{15}-shear piezoelectric response.

References

Al-Ajmi, M. A.; Benjeddou, A. (2008): Damage indications in smart structures using modal effective electromechanical coupling coefficients. *Smart. Mater. Struct.*, vol. 17, 035023.

Araujo, A.; Mota Soares, C. M.; Friedmann, H.; Röhner, J.; Henkel F.-O. (2009): Optimal location of piezoelectric patches and identification of material properties in laminated composite structures. *Proceedings of the 4th ECCOMAS Thematic Conference on Smart Structures and Materials*, Porto, 13-15 July.

Benjeddou, A. (2000): Advances in piezoelectric finite element modeling of adaptive structural elements: a survey. *Comput. Struct.*, vol. 76, pp. 247–363.

Benjeddou, A.; Trindade, M. A.; Ohayon, R. (1997): A unified beam finite element model for extension and shear piezoelectric actuation mechanisms. *J. Intel. Mater. Syst. Struct.*, vol. 8, pp. 1012–1025.

Chevallier, G.; Benjeddou, A. (2009): Couplage électromécanique effectif dans les structures piézoélectriques composites. *Revue des Composites et des Matériaux Avancés*, vol. 19, pp. 239–264.

Chevallier, G.; Ghorbel, S.; Benjeddou, A. (2008): A benchmark for free-vibration and effective coupling of thick piezoelectric smart structures. *Smart. Mater. Struct.*, vol. 17, 065007.

Chevallier, G.; Ghorbel, S.; Benjeddou, A. (2009): Piezoceramic shunted damping concept: testing, modelling and correlation. *Mécanique & Industrie*, vol. 10, pp. 397–411.

Kulikov, G. M.; Plotnikova, S. V. (2008): Geometrically exact four-node piezoelectric solid-shell element. *Mech. Adv. Mater. Struct.*, vol. 15, pp. 199–207.

Trindade, M. A.; Benjeddou, A. (2009): electromechanical coupling coefficients of piezoelectric adaptive structures: critical evaluation and optimization. *Mech. Adv. Mater. Struct.*, vol. 16, pp. 210–223.

Zapfe, J. A.; Lesieutre, G. A. (1999): A discrete layer beam finite element for the dynamic analysis of composite sandwich beams with integral damping layers. *Comput. Struct.*, vol. 70, pp. 647–666.

Appendix

The transformed elastic components for the plate composite ply are defined as follows:

$$\bar{Q}_{11} = Q_{11}\cos^4\theta + Q_{22}\sin^4\theta + 2\left(Q_{12}+2Q_{66}\right)\cos^2\theta\ \sin^2\theta$$

$$\bar{Q}_{22} = Q_{11}\sin^4\theta + Q_{22}\cos^4\theta + 2\left(Q_{12}+2Q_{66}\right)\cos^2\theta\ \sin^2\theta$$

$$\bar{Q}_{12} = Q_{12}\left(\cos^4\theta + \sin^4\theta\right) + \left(Q_{11}+Q_{22}-4Q_{66}\right)\cos^2\theta\ \sin^2\theta$$

$$\bar{Q}_{16} = \left(Q_{11}-Q_{12}-2Q_{66}\right)\cos^3\theta\ \sin\theta - \left(Q_{22}-Q_{12}-2Q_{66}\right)\sin^3\theta\ \cos\theta$$

$$\bar{Q}_{26} = \left(Q_{11}-Q_{12}-2Q_{66}\right)\sin^3\theta\ \cos\theta - \left(Q_{22}-Q_{12}-2Q_{66}\right)\cos^3\theta\ \sin\theta$$

$$\bar{Q}_{16} = (Q_{11} + Q_{22} - 2Q_{12} - 2Q_{66}) \cos^2\theta \ \sin^2\theta + Q_{66}\left(\cos^4\theta + \sin^4\theta\right)$$

$$\bar{Q}_{44} = Q_{44}\cos^2\theta + Q_{55}\sin^2\theta$$

$$\bar{Q}_{55} = Q_{55}\cos^2\theta + Q_{44}\sin^2\theta$$

$$\bar{Q}_{45} = (Q_{55} - Q_{44})\sin\theta\cos\theta$$

Where, θ is the ply angle defined as shown in the following Fig. 6.

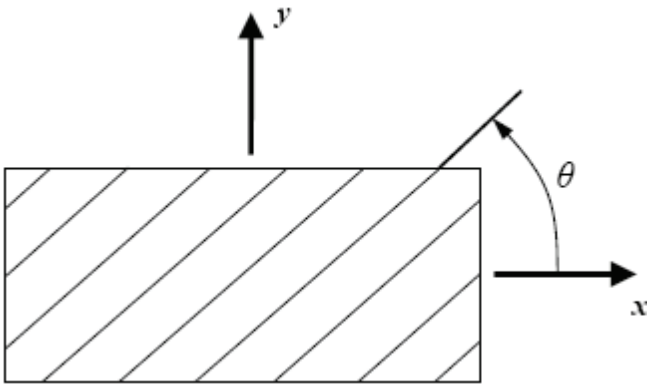

Figure 6: Angle-ply composite layer

The used abbreviations in the text are defined in this list:

1D: one-dimensional
2D: two-dimensional
3D: three-dimensional
DLFE: discrete-layer finite element
DOF(s): degree(s) of freedom
EMCC: electromechanical coupling coefficient
EP: equipotential
FE: finite element
OC: open-circuit
Q9: nine nodes quadrangular
SC: short-circuit